

INITIAL

Copy  
RM L53I23a

NACA RM L53I23a

7478

# NACA

## RESEARCH MEMORANDUM

THE EFFECT OF NOSE RADIUS AND SHAPE ON THE AERODYNAMIC  
CHARACTERISTICS OF A FUSELAGE AND A WING-FUSELAGE  
COMBINATION AT ANGLES OF ATTACK

By John P. Gapcynski and A. Warner Robins

Langley Aeronautical Laboratory  
Langley Field, Va.

NATIONAL ADVISORY COMMITTEE  
FOR AERONAUTICS

WASHINGTON

October 22, 1953

TECH LIBRARY KAFB, NM

0144299



Session 30 1 June 16 Unclassified  
by " " Nas-Tek Rb Hanover (120  
(Ref. to 100-1250 to change) 6-26

By 3 Oct 61

**GRADE OR 0.110L (AKING CHANGE)**

30.11.61  
DATE



0144299

## NATIONAL ADVISORY COMMITTEE FOR AERONAUTICS

## RESEARCH MEMORANDUM

THE EFFECT OF NOSE RADIUS AND SHAPE ON THE AERODYNAMIC  
CHARACTERISTICS OF A FUSELAGE AND A WING-FUSELAGE  
COMBINATION AT ANGLES OF ATTACK

By John P. Gapcynski and A. Warner Robins

## SUMMARY

An investigation has been conducted in the Langley 4- by 4-foot supersonic pressure tunnel to determine the effect of nose blunting on the aerodynamic characteristics of a wing-body combination, and to determine the possible drag reduction of blunt-nosed bodies with the use of spikes and perforated cones. Tests were conducted at a Mach number of 1.61 for an angle-of-attack range of approximately  $-2^{\circ}$  to  $10^{\circ}$ .

Increasing the nose radius while decreasing the nose fineness ratio had little effect on the drag characteristics of the body or wing-body combination for ratios of nose radius to body radius less than 0.4. Above this value the drag increased rapidly with increasing nose radius.

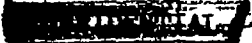
No angle-of-attack effect was noted on the drag increments due to nose blunting except for very blunt nose shapes where the drag increments decreased slightly with increasing angle of attack.

Nose blunting had no interference effects on the drag characteristics of the wing except for extreme degrees of bluntness at the higher angles of attack. In this case, the drag increments due to nose blunting for the wing-body combination were slightly less than those for the body alone.

In comparison to the basic ogival nose, a rearward shift in the center of pressure of the body and wing-body combination and a decrease in the lift coefficient of the body at the higher angles of attack were noted for very large degrees of nose bluntness.

The use of a slotted cone on a blunt-nosed body resulted in large drag reductions.

The drag reduction obtained with the use of spikes varied with the type and length of spike, and the angle of attack. The results obtained



690C 467

with the use of plain spikes were not as favorable as those obtained with oversized conical-headed spikes. This was especially true at the higher angles of attack and for the greater spike lengths.

A large reduction in the drag of a flat-nosed body was obtained with the addition of a conical-headed tripod. An additional decrease was obtained with a tripod covered with 1/4-inch wire mesh.

#### INTRODUCTION

The installation of radar and infrared seeker devices in present-day aircraft and missile configurations has necessitated the use of extremely blunt-nose shapes. Because of this fact, and because the problem does not readily lend itself to theoretical calculations, a great deal of experimental work has been done recently to determine the effect of blunting on the drag characteristics of noses (refs. 1 to 5). The allied problem, that of determining possible ways in which the drag penalties associated with large degrees of nose bluntness may be reduced without impairing the operation of the seeker device, has also received a great deal of attention (refs. 6 to 10).

It has been established that nose shapes with moderate degrees of bluntness may be used without the incurrence of severe drag penalties, and that in some cases, depending upon the Mach number range and nose fineness ratio, a reduction in drag may be obtained for small degrees of bluntness (refs. 3, 4, and 5). Similarly, fairly good drag-reduction characteristics of blunt noses have been obtained with the use of spikes and slotted cones.

The effect of blunt noses on the aerodynamic characteristics of lifting surfaces behind these shapes has not been determined, however, nor have extensive drag data for seeker-type noses been made available at angles of attack other than 0°.

The purpose of the present investigation, therefore, was twofold: first, to determine the effect of nose blunting on the aerodynamic characteristics in pitch of a wing-body combination and, second, to determine the drag-reduction characteristics over an angle-of-attack range of a blunt-nose body equipped with spikes and perforated cones.

Tests were conducted at a Mach number of 1.61 and a Reynolds number per foot of  $4.1 \times 10^6$  in the Langley 4- by 4-foot supersonic pressure tunnel. In addition, limited tests were made at a Mach number of 2.01. The angle-of-attack range was approximately -2° to 10°.

## SYMBOLS

$\rho$	mass density of air	
$V$	airspeed	
$a$	speed of sound in air	
$M$	Mach number, $V/a$	
$q$	dynamic pressure, $\rho V^2/2$	
$\alpha$	angle of attack of body	
$C_D$	drag coefficient, $\text{Drag}/qS_B$	
$C_L$	lift coefficient, $\text{Lift}/qS_B$	
$C_m$	pitching-moment coefficient, $\frac{\text{Pitching moment}}{qS_B L}$	Body alone
$C_{D(W)}$	drag coefficient, $\text{Drag}/qS_W$	
$C_{L(W)}$	lift coefficient, $\text{Lift}/qS_W$	
$C_{m(W)}$	pitching-moment coefficient, $\frac{\text{Pitching moment}}{qS_W \bar{c}}$	Wing-body combination
c.p.	center of pressure	
$S_B$	maximum body cross-sectional area	
$S_W$	wing area	
$L$	length of body	
$\bar{c}$	wing mean aerodynamic chord	
$R$	nose radius	
$R_m$	maximum body radius	
$Re$	Reynolds number	

## MODEL

The basic series of nose shapes (noses 1 to 9) are shown schematically in figure 1. All the nose shapes shown in figure 1 have a 5-inch cylindrical section which is part of the body. Noses 1 to 6 were formed by a successive blunting of a 2.67-fineness-ratio ogive with ratios of nose radius to body radius of 0, 0.15, 0.30, 0.45, 0.70, and 1.00, respectively. Nose 7 was an ogive having a theoretical minimum drag for a given volume and length (see refs. 11 and 12). Noses 8 and 9 (fig. 1(c)) had ratios of nose radius to body radius of 0.15 and 0.30, respectively, but with fineness ratios equal to that of the basic ogive (nose 1). Nose 5 was modified with the addition of a slotted cone (fig. 1(d)) and with different spike shapes of various lengths. The details of the spikes are shown in figure 1(e). Nose 10, figure 1(f), was a flat nose (infinite nose radius). This nose shape was modified with the addition of two separate conical-headed tripods, one of which was covered with 1/4-inch wire mesh.

The wing-body combination used in these tests is shown schematically in figure 2. The body was a circular cylinder 29.25 inches long and 3 inches in diameter. With the basic ogive (nose 1), the overall fineness ratio was 12.4. The wing had a sweepback angle of  $47^\circ$  at the quarter chord, a taper ratio of 0.2, a thickness ratio of 6 percent, aspect ratio of 3.5, and  $\frac{1}{3} - \frac{1}{3} - \frac{1}{3}$  symmetrical hexagonal airfoil sections.

## TESTS

The test program was divided into two parts: first, the body and wing-body combination were tested with noses 1 to 9, to determine the effect of nose blunting on the aerodynamic characteristics of these configurations; and, second, the body alone was tested with the slotted cone, spikes, and tripods to determine the drag-reduction characteristics of these devices. All these tests were conducted at a Mach number of 1.61. In addition, both the body and the wing-body combination were tested with noses 1 and 6 at a Mach number of 2.01. The angle-of-attack range was approximately  $-2^\circ$  to  $10^\circ$ .

The tunnel stagnation conditions for  $M = 1.61$  were: pressure 14.34 pounds per square inch, temperature  $100^\circ$  F, dew point approximately  $-35^\circ$  F. At a Mach number of 2.01, tunnel pressure was maintained at 14.6 pounds per square inch and stagnation temperature at  $95^\circ$  F. The Reynolds number per foot was  $4.1 \times 10^6$  for  $M = 1.61$  and  $3.7 \times 10^6$  for  $M = 2.01$ .

Lift, drag, and moment measurements were obtained with an internal strain-gage balance.

Base-pressure measurements were obtained from a pressure orifice located on the model sting. In order to minimize the effects of base-pressure variations on the chord-force measurements, a sting block with a diameter equal to that of the fuselage was fitted to the supporting sting close to the model base.

A small mirror was mounted on the model so that the angle of attack could be measured optically during each test.

The accuracy of the values of drag coefficient, based on maximum body cross-sectional area is  $\pm 0.01$ .

## RESULTS

The experimental data for each configuration are presented in terms of the variation of lift, drag, and moment coefficients and center-of-pressure location with angle of attack. For the wing-body combination, the lift-drag-ratio variation is also presented. The aerodynamic coefficients for the body-alone tests are based on maximum body cross-sectional area and body length, and the coefficients for the wing-body combination are based on wing area and mean aerodynamic chord. Moments are presented about a point 4.24 body diameters ahead of the base. For the wing-body combination, this point is at the quarter-chord point of the mean aerodynamic chord of the wing.

The aerodynamic characteristics of the body and wing-body combination in pitch for noses 1 to 9 are presented in figures 3 and 4, respectively.

The drag increments due to nose blunting for the body and wing-body combination are presented in figure 5. These increments represent the difference in drag of a configuration with an ogival nose (nose 1) and a configuration with a blunt nose (noses 2 to 6). The tailed symbols represent data obtained at a Mach number of 2.01.

The prediction of the drag increments at  $0^\circ$  angle of attack, as shown by the curve " $\Delta C_D$  Estimation" in figure 5, was obtained from an estimation of the wave drag and skin-friction drag of each nose shape. The wave drag was obtained from a combination of the experimental pressure distribution over a sphere (ref. 13), and the theoretical pressure distribution over an ogive (ref. 14). The viscous drag was obtained by using the skin-friction coefficient for laminar flow over a flat plate at a Mach number of 1.61 (ref. 15). This value was  $C_f = 1.315/\sqrt{Re}$ .

The values of the skin-friction coefficient were increased by 12 percent to account for the correction from a flat plate to a body of revolution. (Mangler's transformation applied to a parabolic body.)

The data shown in figure 6 represent the variation of the aerodynamic characteristics of a blunt-nosed body equipped with a slotted nose cone. In figure 7, data are presented for the same body equipped with various types and lengths of nose spikes. The effect of spike length and angle of attack on the drag characteristics of the body is presented in detail in figure 8.

The aerodynamic characteristics of a flat-nosed body with and without tripod nose sections are presented in figure 9.

#### DISCUSSION

In general, there was no effect of nose blunting on the lift, moment, or center-of-pressure characteristics of either the body or wing-body combination, except for extreme degrees of bluntness (figs. 3 and 4). The addition of the full hemispherical nose (nose 6) resulted in a rearward shift in the center of pressure for both the body and wing-body combination, and a decrease in the lift coefficient of the body alone at the higher angles of attack. Center-of-pressure values for the body alone have not been presented in the low angle-of-attack range, since widely varying results were obtained with small variations in lift coefficient.

The effects of nose blunting on the drag characteristics of the body and wing-body combination may be noted in figure 5. The addition of moderate degrees of bluntness, that is, ratios of nose radius to body radius  $R/R_m$ , up to the order of 0.4, had little detrimental effect on the drag characteristics. For values of  $R/R_m$  greater than 0.4, however, the drag increased appreciably. Although a slight decrease in drag may be noted for small degrees of nose bluntness, this effect is within the accuracy of the data and may be questionable.

There was no angle-of-attack effect on the drag increments except for extreme degrees of bluntness (nose 6). In this case, the drag increments decreased slightly with increasing angle of attack. This effect may also be noted for a Mach number of 2.01.

One important result which may be noted from the data of figure 5 is that, with the exception of nose 6 ( $R/R_m = 1$ ), the drag increments due to nose blunting for the body alone were equal to those for the wing-body combination. For nose 6, the increments for the body alone were

greater than those for the wing-body combination, and this difference increased as the angle of attack was increased.

The prediction of the drag increments of the body alone at  $0^{\circ}$  angle of attack was in fair agreement with the experimental results. In the determination of these values a laminar skin-friction coefficient was used. With the exception of the body with the full hemispherical nose (nose 6), schlieren photographs of the flow indicated that boundary-layer transition from a laminar to a turbulent state at  $0^{\circ}$  angle of attack occurred at approximately 6 body diameters ahead of the base of the model. For nose 6, the boundary layer was turbulent over the complete cylindrical portion of the body.

In order to establish the effects of nose fineness ratio on the drag increments due to blunting, noses 8 and 9 were tested and the results compared with the drag increments obtained with noses 2 and 3, respectively. No differences in these drag increments were noted.

A small reduction in the drag of the body and wing-body combination resulted from use of the minimum-drag ogive (nose 7). This drag reduction was evident throughout the angle-of-attack range.

The addition of the slotted cone and spikes to a blunt-nosed body (body plus nose 5) had no appreciable effect on the lift, moment, and center-of-pressure characteristics of this configuration (figs. 6 and 7). Large decreases in drag throughout the angle-of-attack range were obtained with the slotted cone. The drag reduction obtained with spikes varied with the type and length of spike, and the angle of attack (figs. 7 and 8).

For the plain spikes at  $0^{\circ}$  angle of attack, the drag decreased with increasing spike length up to the maximum length tested. This variation was approximately linear. With increase in angle of attack, the spike length giving minimum drag decreased. This change occurred rather abruptly between  $2^{\circ}$  and  $4^{\circ}$  angle of attack for the body with the greatest spike length and may be associated with a rearward shift of the point of separation of the boundary layer on the spike. This effect was not noted for the case of the conical-headed spikes, which gave somewhat better drag-reduction characteristics than the plain spikes throughout the angle-of-attack range.

The flat-nosed body was tested at the request of the Pilotless Aircraft Research Division to determine the drag-reduction characteristics of tripods covered with wire mesh. This type of nose shape, if practical from the drag standpoint, would provide for an inexpensive nose shape in actual missile manufacture. Large reductions in the drag of the flat-nosed body (fig. 9) were obtained with the addition of the tripods.

## CONCLUDING REMARKS

An investigation has been conducted in the Langley 4- by 4-foot supersonic pressure tunnel to determine the effect of nose blunting on the aerodynamic characteristics of a wing-body combination, and to determine the possible drag reduction of blunt-nosed bodies with the use of spikes and perforated cones. Tests were conducted at a Mach number of 1.61 and a Reynolds number per foot of  $4.1 \times 10^6$ . A few tests were made at a Mach number of 2.01. The angle-of-attack range was approximately  $-2^\circ$  to  $10^\circ$ .

Increasing the nose radius while decreasing the nose fineness ratio had little effect on the drag characteristics of the body or wing-body combination for ratios of nose radius to body radius less than 0.4. Above this value the drag increased rapidly with increasing nose radius. A comparison of these results with the results of limited tests of nose shapes having a constant fineness ratio with increasing nose radius indicated that there was no effect of fineness ratio on the drag characteristics of blunt nose shapes. A reduction in the drag of the body and wing-body combination throughout the angle-of-attack range was obtained with a minimum-drag nose shape (Von Kármán ogive for a given length and volume).

No angle-of-attack effect was noted on the drag increments due to nose blunting except for extremely blunt nose shapes where the drag increments decreased slightly with increasing angle of attack.

Nose blunting had no interference effects on the drag characteristics of the wing except for very blunt nose shapes at the higher angles of attack. For a ratio of nose radius to body radius of 1.0, the drag increments due to nose blunting for the wing-body combination were slightly less than those for the body alone.

In comparison to the basic ogival nose, a rearward shift in the center of pressure of the body and wing-body combination, and a decrease in the lift coefficient of the body at the higher angles of attack were noted for very large degrees of nose bluntness.

The use of a slotted cone on a blunt-nosed body resulted in large drag reductions. At  $0^\circ$  angle of attack the drag increment due to nose blunting was reduced approximately 75 percent with the addition of the slotted cone.

The drag reduction obtained with the use of spikes varied with the type and length of spike, and the angle of attack. The results obtained with the use of plain spikes were not as favorable as those obtained with oversized conical-headed spikes. This was especially true at the higher

angles of attack and for the greater spike lengths. In each case, the magnitude of the drag reduction decreased with increasing angle of attack. The optimum plain spike length decreased with increase in angle of attack.

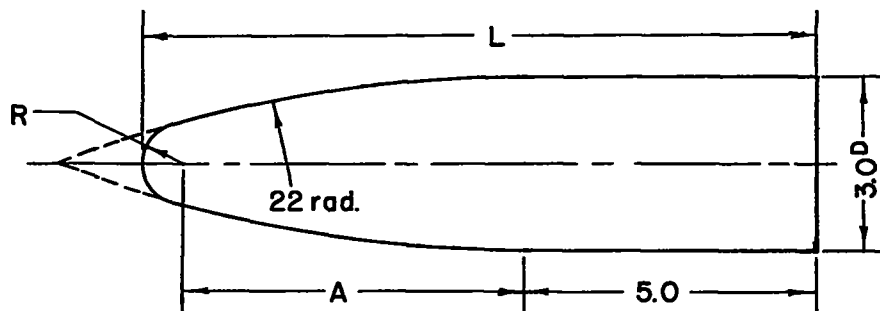
A large reduction in the drag of the flat-nosed body was obtained with the addition of a conical-headed tripod. An additional decrease was obtained with a tripod covered with 1/4-inch wire mesh.

Langley Aeronautical Laboratory,  
National Advisory Committee for Aeronautics,  
Langley Field, Va., September 9, 1953.

## REFERENCES

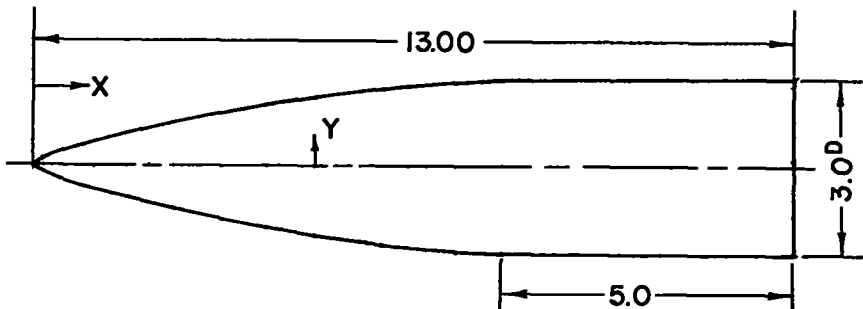
1. Hart, Roger G.: Flight Investigation of the Drag of Round-Nosed Bodies of Revolution at Mach Numbers From 0.6 to 1.5 Using Rocket-Propelled Test Vehicles. NACA RM L51E25, 1951.
2. Wallskog, Harvey A., and Hart, Roger G.: Investigation of the Drag of Blunt-Nosed Bodies of Revolution in Free Flight at Mach Numbers from 0.6 to 2.3. NACA RM L53D14a, 1953.
3. Perkins, Edward W., and Jorgensen, Leland H.: Investigation of the Drag of Various Axially Symmetric Nose Shapes of Fineness Ratio 3 for Mach Numbers From 1.24 to 3.67. NACA RM A52H28, 1952.
4. Sommer, Simon C., and Stark, James A.: The Effect of Bluntness on the Drag of Spherical-Tipped Truncated Cones of Fineness Ratio 3 at Mach Numbers 1.2 to 7.4. NACA RM A52B13, 1952.
5. Seiff, Alvin, Sandahl, Carl A., Chapman, Dean R., Perkins, E. W., and Gowen, F. E.: Aerodynamic Characteristics of Bodies at Supersonic Speeds. A Collection of Three Papers. NACA RM A51J25, 1951.
6. Piland, Robert O.: Preliminary Free-Flight Investigation of the Zero-Lift Drag Penalties of Several Missile Nose Shapes for Infrared Seeking Devices. NACA RM L52F23, 1952.
7. Jones, Jim J.: Flow Separation From Rods Ahead of Blunt Noses at Mach Number 2.72. NACA RM L52E05a, 1952.
8. Platou, A. S.: Body Nose Shapes for Obtaining High Static Stability. Memo. Rep. No. 592. Ballistic Res. Labs., Aberdeen Proving Ground, Feb. 1952.
9. Robins, A. Warner: Preliminary Investigation of the Effect of Several Seeker-Nose Configurations on the Longitudinal Characteristics of a Canard-Type Missile at a Mach Number of 1.60. NACA RM L53I18, 1953.
10. Mair, W. A.: Experiments on Separation of Boundary Layers on Probes in Front of Blunt-Nosed Bodies in a Supersonic Air Stream. Phil. Mag., ser. 7, vol. 43, no. 342, July 1952, pp. 695-716.
11. Von Kármán, Theodore: The Problem of Resistance in Compressible Fluids. GALCIT Pub. No. 75, 1936. (From R. Accad. d'Italia, Cl. Sci. Fis., Mat. e Nat., vol. XIV, 1936.)

12. Sears, William R.: On Projectiles of Minimum Wave Drag. Quarterly Appl. Math., vol. IV, no. 4, Jan. 1947, pp. 361-366.
13. Gooderum, Paul B., and Wood, George P.: Density Fields Around a Sphere at Mach Numbers 1.30 and 1.62. NACA TN 2173, 1950.
14. Van Dyke, Milton Denaan: Practical Calculation of Second-Order Supersonic Flow Past Nonlifting Bodies of Revolution. NACA TN 2744, 1952.
15. Klunker, E. B., and McLean, F. Edward: Laminar Friction and Heat Transfer at Mach Numbers From 1 to 10. NACA TN 2499, 1951.



Nose	$L$	$A$	$R$	$R/R_m$
1	13.00	8.00	0	0
2	12.57	7.34	.23	.15
3	12.10	6.65	.45	.30
4	11.55	5.87	.68	.45
5	10.37	4.32	1.05	.70
6	6.50	0	1.50	1.00

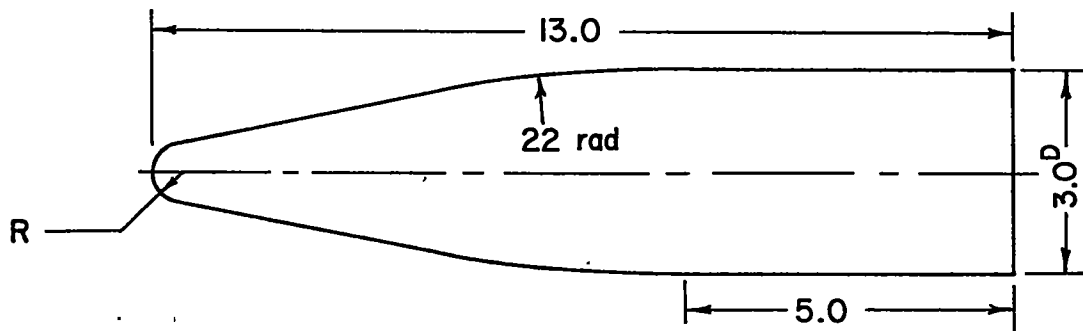
(a) Noses 1 to 6.



Coordinates			
$X$	$Y$	$X$	$Y$
0	0	3.20	.917
.16	.104	4.00	1.061
.32	.174	4.80	1.187
.48	.235	5.60	1.297
.80	.343	6.40	1.389
1.60	.566	7.20	1.461
2.40	.754	8.00	1.500

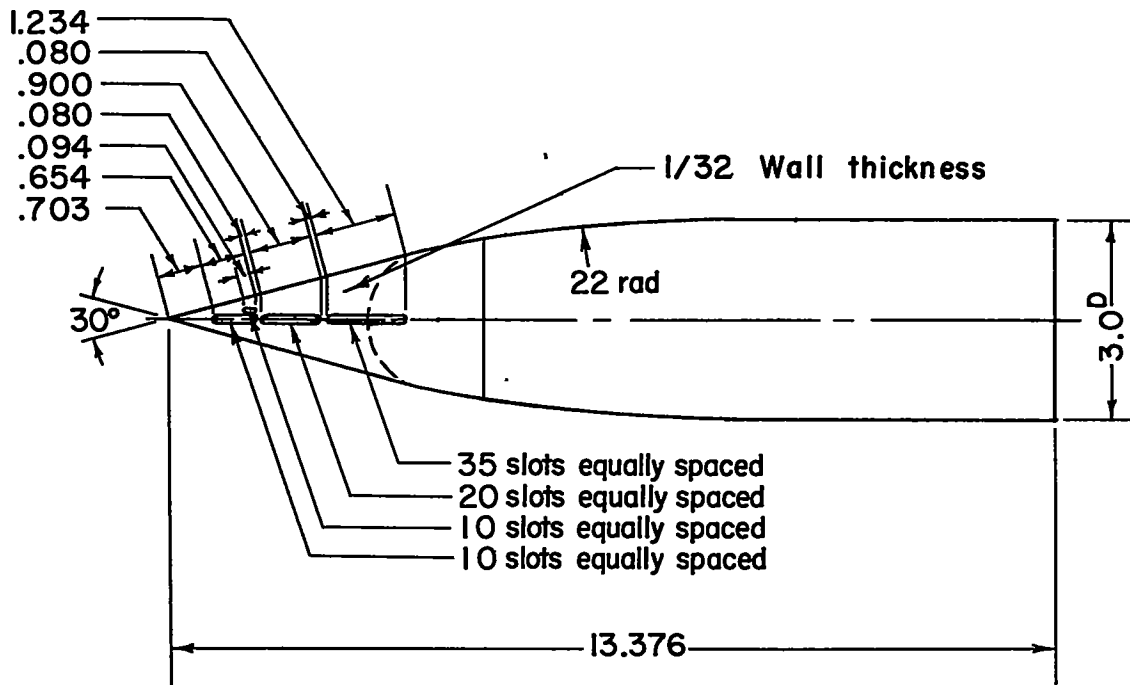
(b) Nose 7.

Figure 1.- Details of model nose shapes. All dimensions in inches.



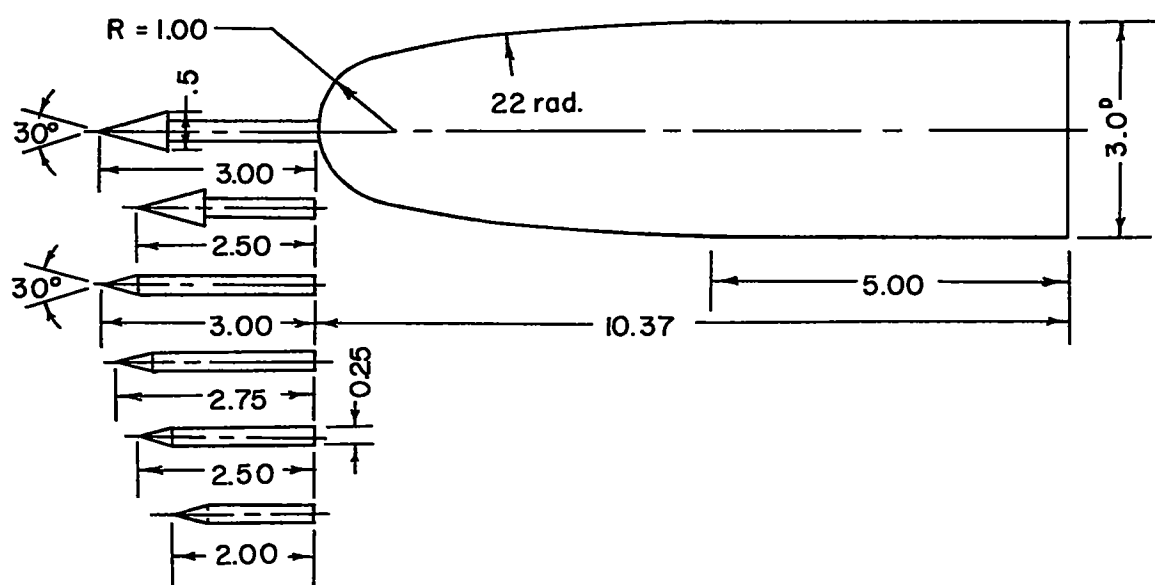
Nose	R	$R/R_m$
8	.23	.15
9	.45	.30

(c) Noses 8 and 9.

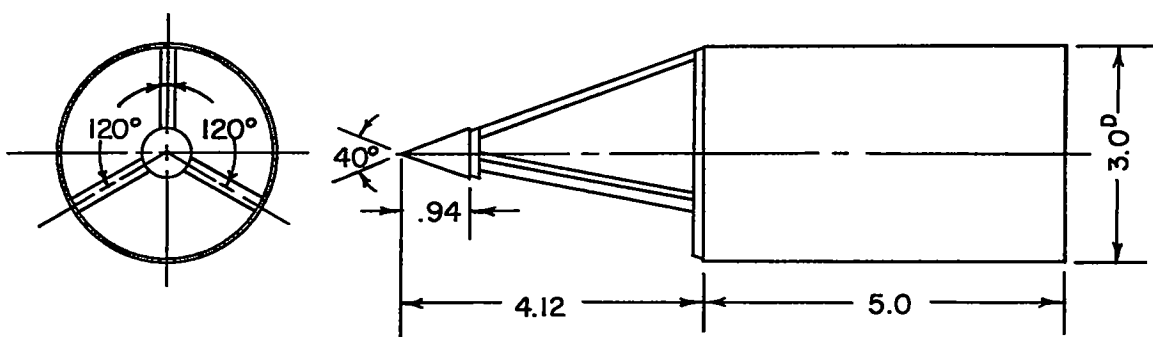


(d) Slotted cone.

Figure 1.- Continued.



(e) Spike details.



(f) Nose 10.

Figure 1.- Concluded.

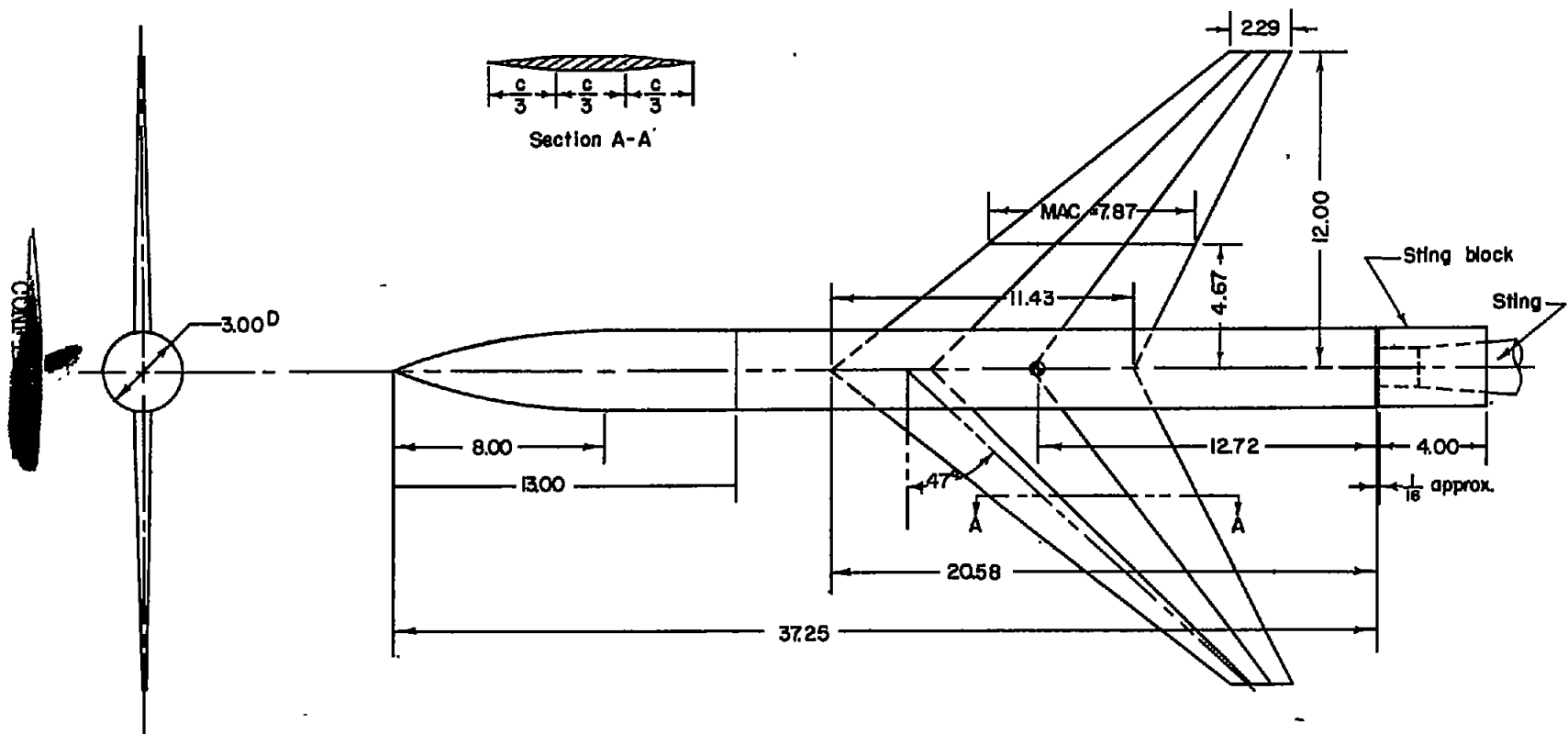


Figure 2.-- Schematic layout of wing-body combination. All dimensions in inches unless otherwise specified.

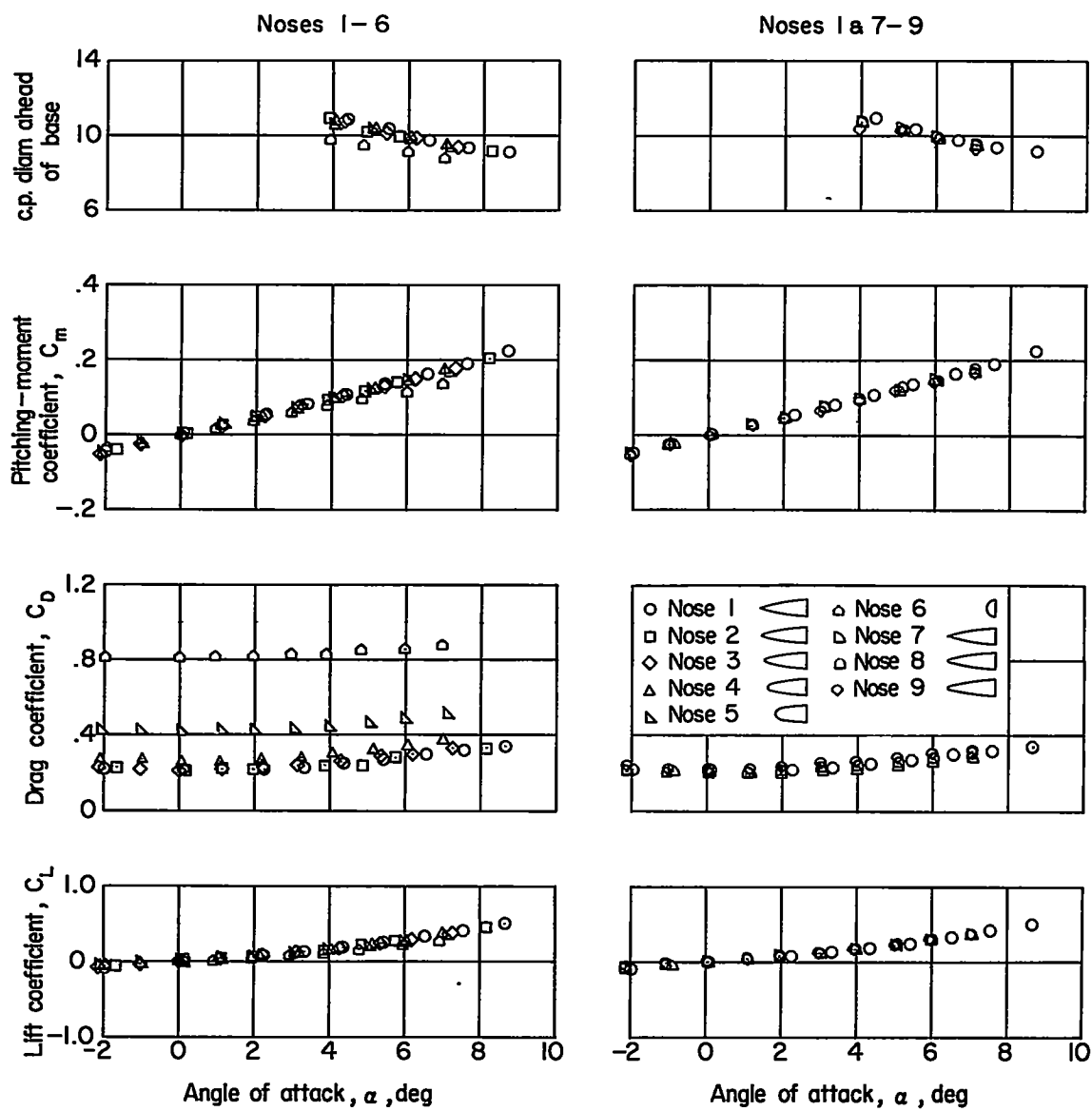


Figure 3.- Variation of the aerodynamic characteristics of a body of revolution with angle of attack for various nose shapes.  $M = 1.61$ .

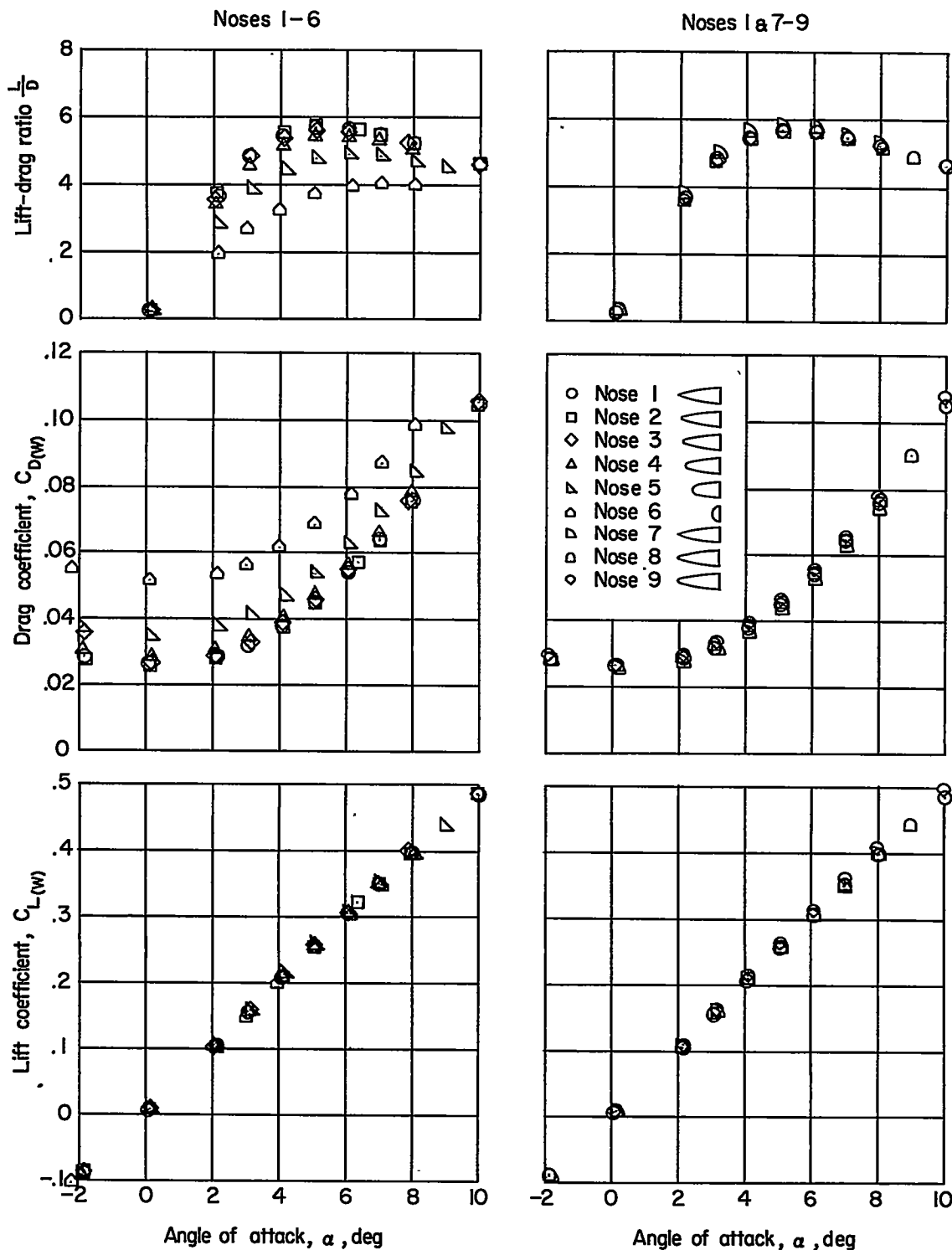


Figure 4.- Variation of the aerodynamic characteristics of a wing-body combination with angle of attack for various nose shapes.  $M = 1.61$ .

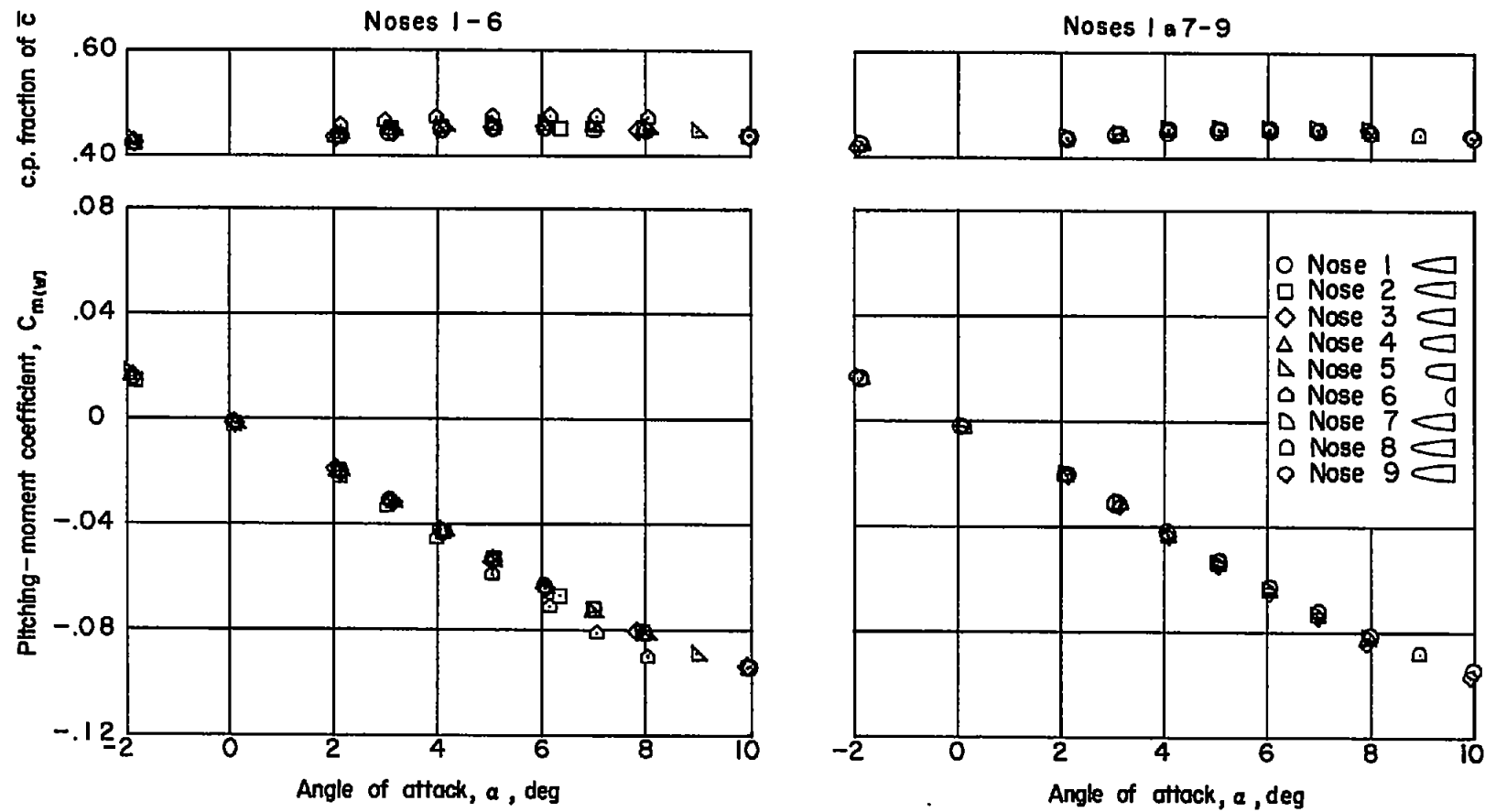


Figure 4.- Concluded.

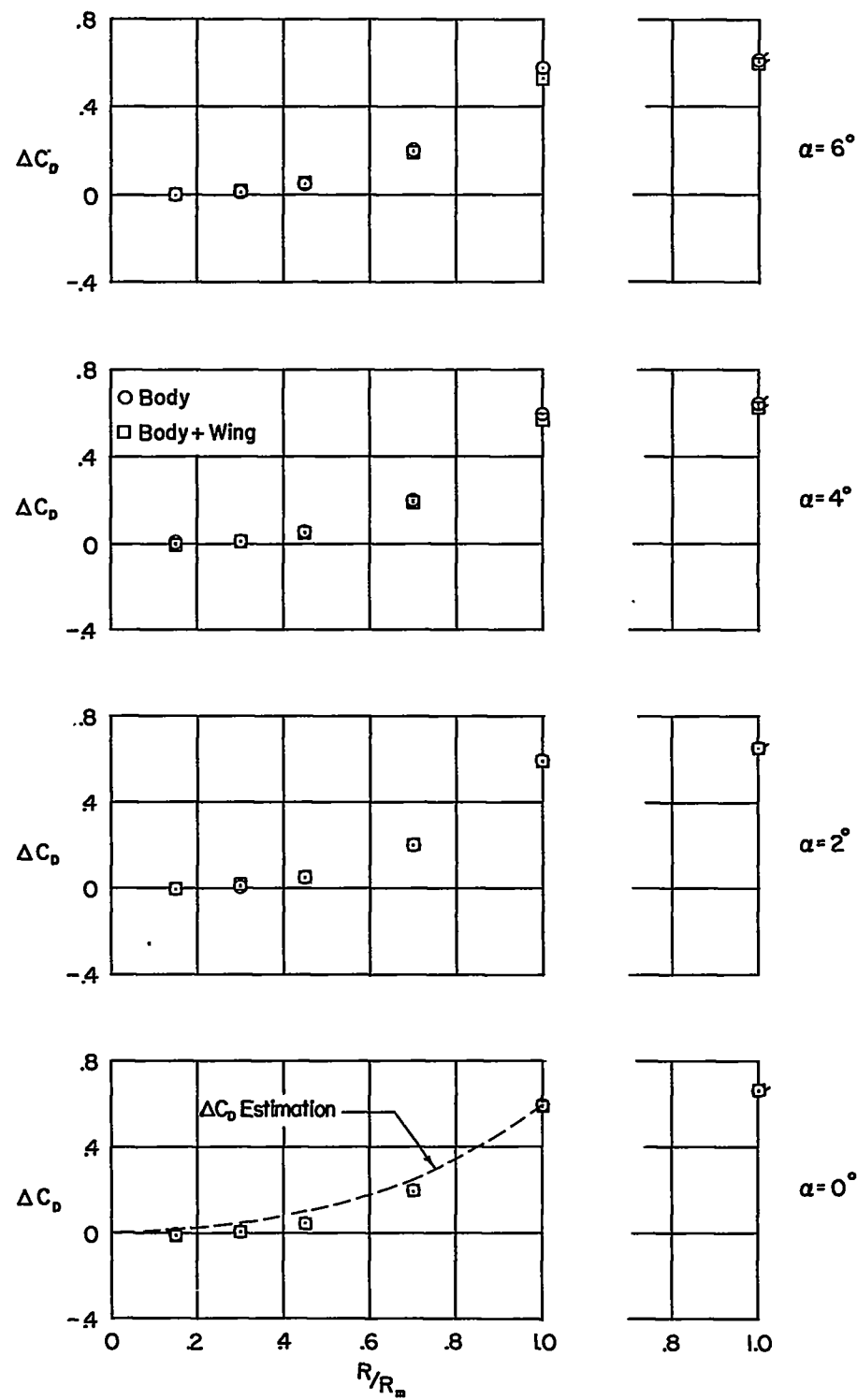


Figure 5.- Variation of the drag increment due to nose blunting with nose radius for various angles of attack. Tailed symbols refer to data obtained at  $M = 2.01$ .

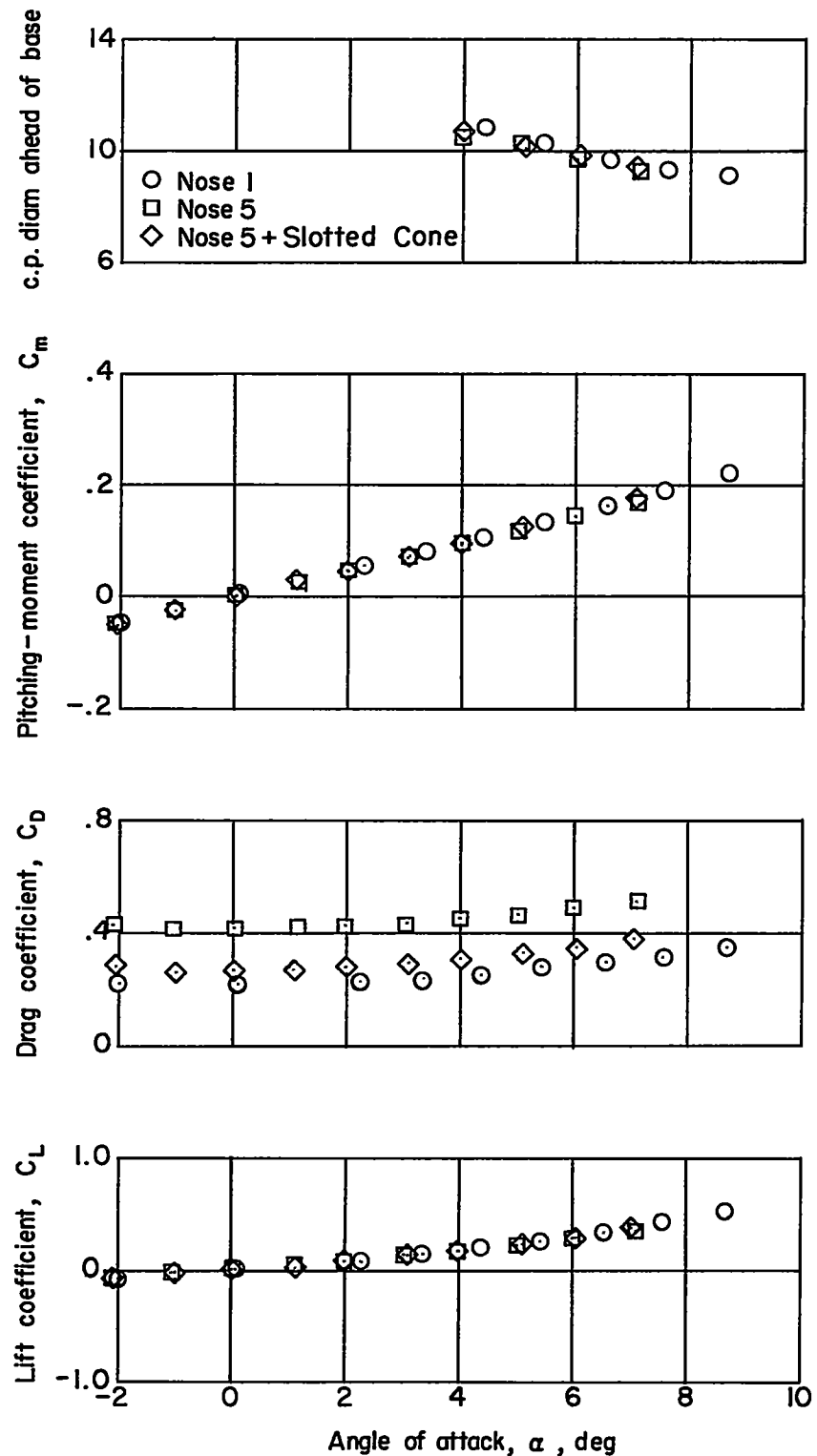


Figure 6.- Variation of the aerodynamic characteristics of a body of revolution with angle of attack for various nose shapes.

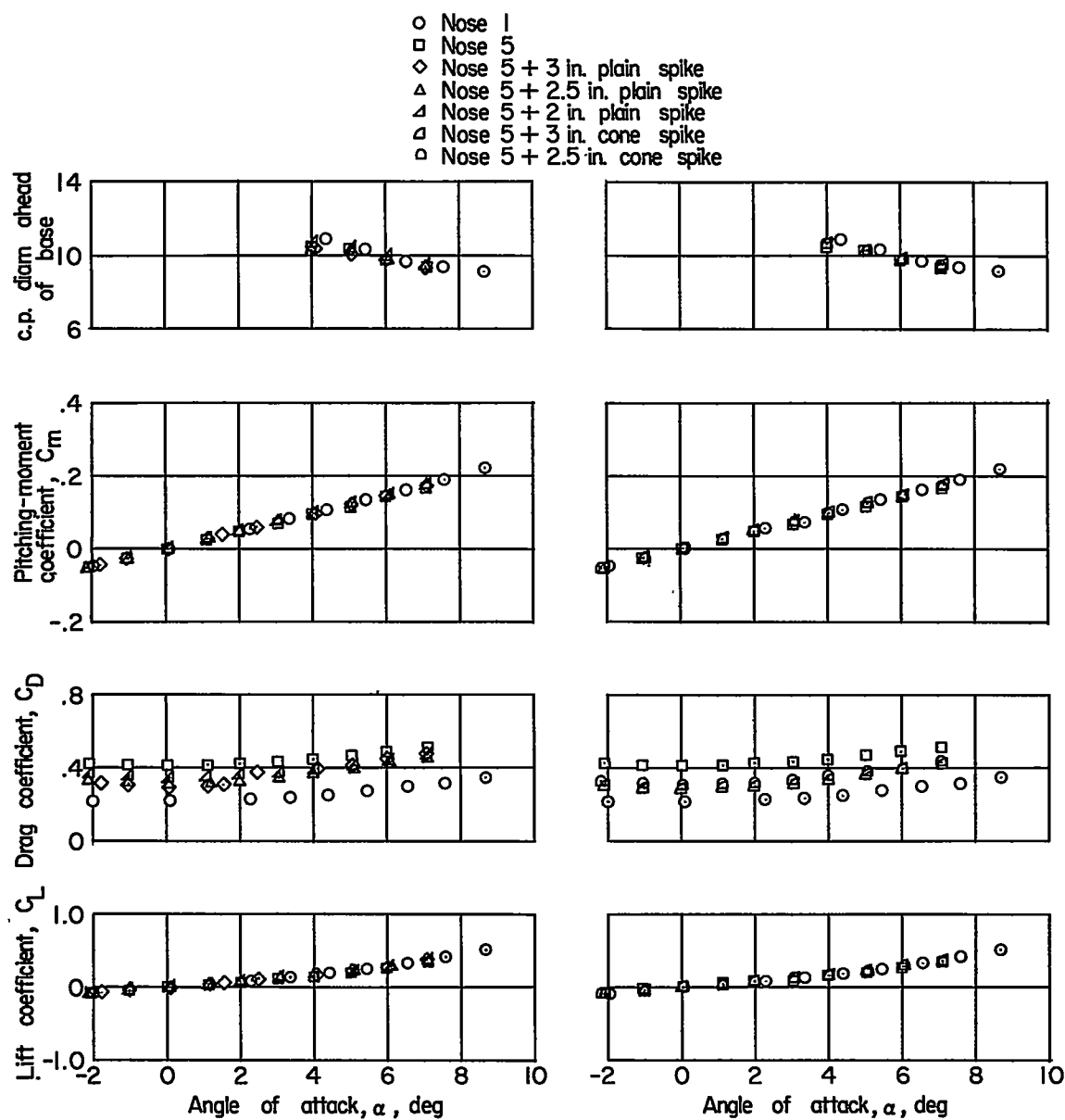


Figure 7.- Variation of the aerodynamic characteristics of a body of revolution with angle of attack for various types and lengths of nose spikes.

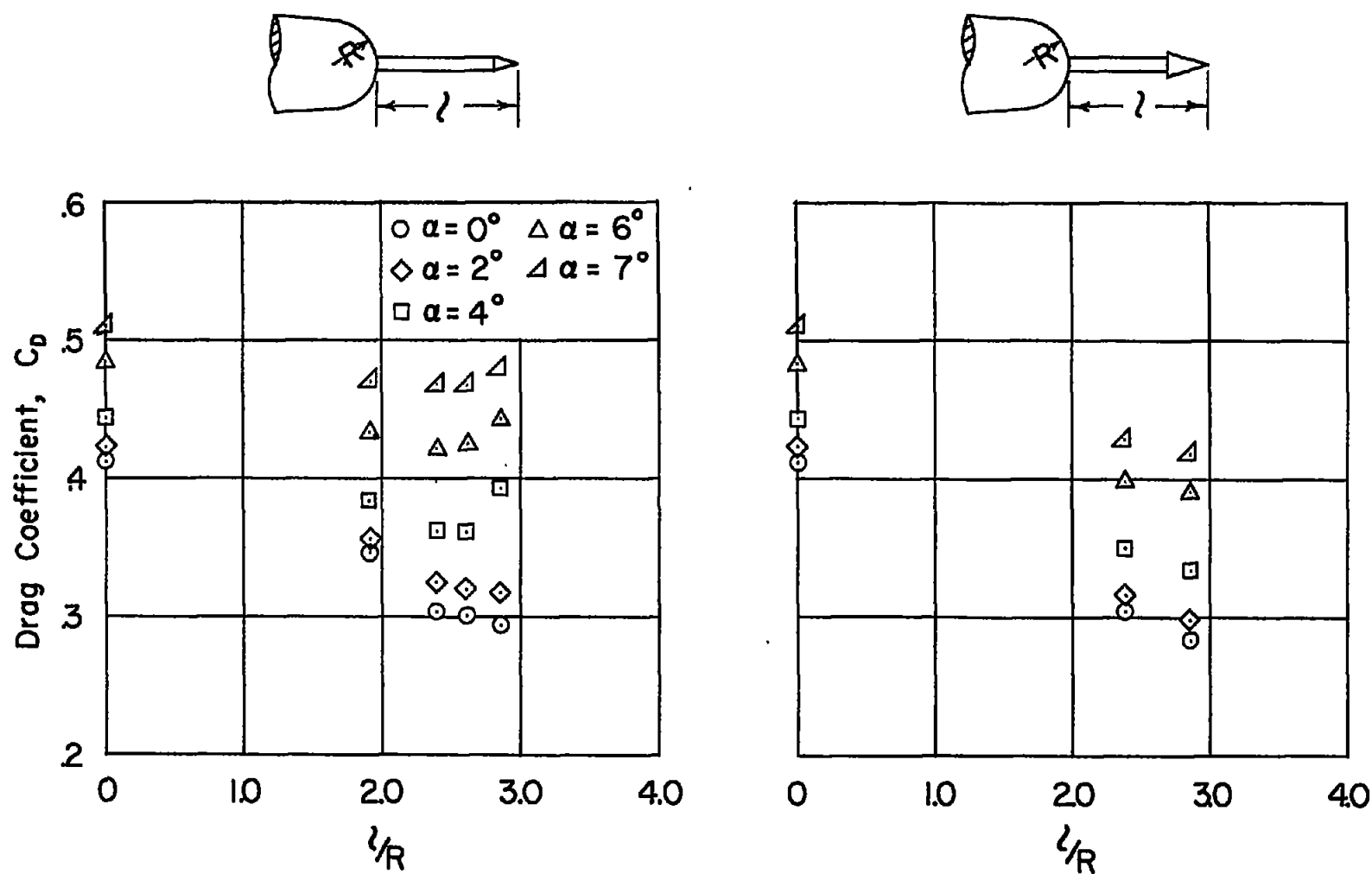


Figure 8.- Effect of the variation of nose-spike length and angle of attack on the drag characteristics of a blunt-nosed body of revolution. (Body + nose 5.)

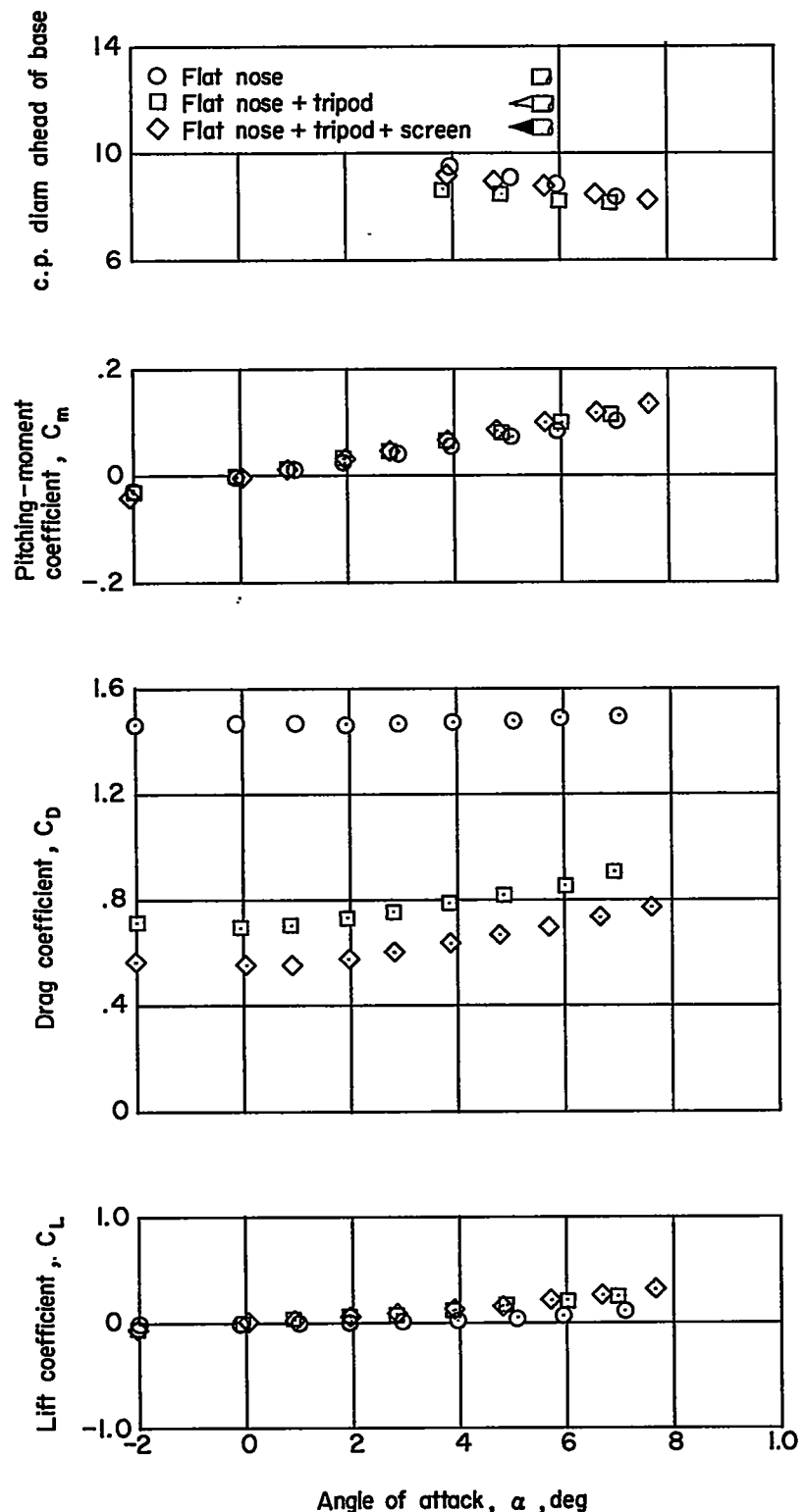


Figure 9.- Variation of the aerodynamic characteristics of a body of revolution with angle of attack for various nose shapes.